



Virtual histology of multi-modal magnetic resonance imaging of cerebral cortex in young men

Yash Patel^{a,b}, Jean Shin^c, Mark Drakesmith^d, John Evans^d, Zdenka Pausova^{c,e}, Tomas Paus^{b,f,*}

^a Institute of Medical Sciences, University of Toronto, Toronto, ON, Canada

^b Bloorview Research Institute, Holland Bloorview Kids Rehabilitation Hospital, Toronto, ON, Canada

^c The Hospital for Sick Children, Toronto, ON, Canada

^d CUBRIC, School of Psychology, Cardiff University, Cardiff, UK

^e Departments of Physiology and Nutritional Sciences, University of Toronto, Toronto, ON, Canada

^f Departments of Psychology and Psychiatry, University of Toronto, Toronto, ON, Canada

ARTICLE INFO

Keywords:

Magnetic resonance imaging
Myelin water fraction
Relaxometry
Cerebral cortex
mcDESPOT imaging
Diffusion tensor imaging
ALSPAC

ABSTRACT

Neurobiology underlying inter-regional variations - across the human cerebral cortex - in measures derived with multi-modal magnetic resonance imaging (MRI) is poorly understood. Here, we characterize inter-regional variations in a large number of such measures, including T1 and T2 relaxation times, myelin water fraction (MWF), T1w/T2w ratio, mean diffusivity (MD), fractional anisotropy (FA), magnetization transfer ratio (MTR) and cortical thickness. We then employ a virtual-histology approach and relate these inter-regional profiles to those in cell-specific gene expression. Virtual histology revealed that most MRI-derived measures, including T1, T2 relaxation time, MWF, T1w/T2w ratio, MTR, FA and cortical thickness, are associated with expression profiles of genes specific to CA1 pyramidal cells; these genes are enriched in biological processes related to dendritic arborisation. In addition, T2 relaxation time, MWF and T1w/T2w ratio are associated with oligodendrocyte-specific gene-expression profiles, supporting their use as measures *sensitive* to intra-cortical myelin. MWF contributes more variance than T1w/T2w ratio to the mean oligodendrocyte expression profile, suggesting greater sensitivity to myelin. These cell-specific MRI associations may help provide a framework for determining which MRI sequences to acquire in studies with specific neurobiological hypotheses.

1. Introduction

A key challenge in neuroimaging is our limited understanding of the neurobiology underlying various measures derived with magnetic resonance imaging (MRI). Studies bridging the gap between *in vivo* MRI and *ex vivo* histology represent one way of addressing this challenge (Eickhoff et al., 2005) and, in turn, facilitate the interpretation of changes in these measures observed, for example, during development (Giedd et al., 1999) and aging (Walhovd et al., 2016), or across various clinical populations (Thompson et al., 2019). The human cerebral cortex has a complex cellular composition, both in terms of cell types (neurons & glia) and neuropil (dendrites, axons), the latter found in between cell bodies (Braitenberg and Schüz, 2013). There are a handful of histological studies showing prolonged intracortical myelination continuing up to the third decade of life (Miller et al., 2012). This complexity of cellular composition adds to the difficulty in the interpretation of MR findings

with regard to the possible cellular processes underlying inter-individual differences observed *in vivo*. Advances in MRI have led to the development of MR sequences sensitive to varying microstructural elements within the cerebral cortex (Edwards et al., 2018). Here, we use a virtual histology approach (Shin et al., 2017) to explore the neurobiological underpinnings of inter-regional variations of several MRI measures, including T1 and T2 relaxation times, myelin water fraction (MWF), magnetization transfer ratio (MTR), T1w/T2w, fractional anisotropy (FA), mean diffusivity (MD) and cortical thickness across the human cerebral cortex. By relating gene-expression data from the Allen Human Brain Atlas (Hawrylycz et al., 2012), and cell-specific marker information from single-cell RNA sequencing (Zeisel et al., 2015), we assess cellular correlates of these measures within the cerebral cortex to aid their interpretation in future studies.

A large number of MR modalities, such as quantitative T1 and T2 imaging, and diffusion weighted imaging, are available for probing

* Corresponding author. Bloorview Research Institute, Holland Bloorview Kids Rehabilitation Hospital, Toronto, ON, Canada.

E-mail address: tpaus@hollandbloorview.ca (T. Paus).

<https://doi.org/10.1016/j.neuroimage.2020.116968>

Received 27 November 2019; Received in revised form 2 May 2020; Accepted 14 May 2020

Available online 22 May 2020

1053-8119/© 2020 The Author(s). Published by Elsevier Inc. This is an open access article under the CC BY-NC-ND license (<http://creativecommons.org/licenses/by-nc-nd/4.0/>).

structural properties of the human cerebral cortex (Edwards et al., 2018; Laule et al., 2007). All of these modalities generate MR contrast across cortical regions (and lamina) that reflects variations in the chemical and physical environments of protons in the tissue. In the cerebral cortex, such inter-regional variations in MR contrast may – to some extent – reflect variations in cortical cytoarchitecture and myeloarchitecture (Eickhoff et al., 2005). Quantitative T1 measures the time it takes to recover longitudinal magnetization following a radiofrequency (RF) inversion (Tofts, 2003). Within the cerebral cortex, T1 is sensitive to changes in water content (Gelman et al., 2001; Kamman et al., 1988), iron content (Edwards et al., 2018), myelin (Eickhoff et al., 2005; Lutti et al., 2014; Reeves et al., 2016) and overarching microstructure (Bernhardt et al., 2018; Gracien et al., 2016; Parry et al., 2003). Quantitative T2 measures the time it takes to decay transverse magnetization (transverse phase coherence) induced by an RF-pulse. Similar to T1, T2 is also sensitive to iron content (Edwards et al., 2018) and histologically measured intra-cortical myelin (Reeves et al., 2016). Multi-echo T2 relaxation distinguishes two types of water, a short T2 component (~20 ms) thought to originate from water trapped between layers of myelin sheaths, and a longer T2 component (~100 ms) representing intra-/extracellular water (Laule et al., 2007). A measure of myelin content, namely the myelin water fraction (MWF), can be constructed by creating a ratio of the signal area of short T2 (myelin water) divided by the total T2 signal area; MWF is highly correlated with myelin content assessed histologically in tissues obtained from patients with multiple sclerosis (MS), including gray matter, white matter and sections including MS lesions ($R^2 = 0.67$, $n = 25$; Laule et al., 2006).

Another measure thought to be sensitive to intracortical myelination, namely T1w/T2w ratio, was proposed by (Glasser and Van Essen, 2011) based on their observation of a strong (spatial) correlation between histologically derived myelin maps and MR-derived T1w/T2w ratio maps (Glasser et al., 2014). There is some controversy, however, regarding the use of T1w/T2w as a “myelin map”. For instance, T1w/T2w ratio was sensitive to dendrite density but not myelin content in *post mortem* tissue samples from patients with multiple sclerosis (Righart et al., 2017).

Magnetization transfer ratio is an indirect measure of macromolecular density; it depends on the transfer of spin between bound and free protons (De Boer, 1995). Bound protons are restricted in their movement (e.g., when part of large molecules) while free protons are unrestricted (water). Historically, MTR has been used as a myelin measure within white matter (Schmierer et al., 2004), and is believed to hold the same sensitivity to myelin in cortical gray matter (Chen et al., 2013; Edwards et al., 2018; Laule et al., 2007). We should keep in mind, however, that MTR is not necessarily specific to myelin, as there may be other under-appreciated sources of signal from macromolecules, such as cellular membranes of neurites (Laule et al., 2007; Uematsu et al., 2004). Histological examinations in demyelinating mouse models fail to show a relationship between MTR and myelin content in white matter, deep gray-matter, and cortical gray-matter (Fjær et al., 2015).

Diffusion weighted imaging (DWI) characterizes the diffusion of water within tissue – probing “microstructural” organization of brain tissue (axons, neurites, and cellular projections). Single-shell DWI modelled using a diffusion tensor model (DTI) provides two key measures characterizing the movement of water, namely fractional anisotropy and mean diffusivity (Mori and Barker, 1999). Fractional anisotropy (FA), a measure of how directional (or anisotropic) the motion of water is in a given voxel, has been used to infer changes in dendritic arbor during development (Huang et al., 2008; Ouyang et al., 2019), and axonal degeneration in the cerebral cortex of patients with multiple sclerosis (Preziosa et al., 2019). Mean diffusivity (MD) measures the average motion of water, and is commonly used to detect pathological changes in tissue microstructure (Cercignani et al., 2001; Tuor et al., 2014).

Finally, we investigate neurobiological correlates in cortical thickness as it is a dynamic measure used to characterize changes in cortical structure across the lifespan (Walhovd et al., 2016), and across various clinical conditions (Thompson et al., 2019) in large datasets.

2. Methods

2.1. Participants

Participants in this study were recruited from the Avon Longitudinal Study of Parents and Children (ALSPAC: <http://www.alspac.bris.ac.uk>). This is a birth cohort designed to investigate the influence of various factors on health trajectories. Pregnant women residing in the former Avon Health Authority in South-West England, who had an estimated date of delivery between 1 April 1991 and 31 December 1992, were invited to participate in the study. This resulted in a cohort of 14,541 pregnancies (Boyd et al., 2013; Fraser et al., 2013). Ethical approval for the study was obtained from the ALSPAC Law and Ethics Committee and the Local Research Ethics Committees. Informed consent for the use of data collected via questionnaires and clinics was obtained from participants following the recommendations of the ALSPAC Ethics and Law Committee at the time. Please note that the study website contains details of all the data that are available through a fully searchable data dictionary and variable search tool (<http://www.bristol.ac.uk/alspac/researchers/our-data/>).

Brain imaging was carried out in a subsample of 507 young men when they were 18–21.5 years old. Only men were scanned owing to the focus of the NIH grant funding this work. Participants were selected based on their domicile being within a 3-h journey (one-way) from the scanning site, and availability of three or more longitudinal samples of blood used for measuring levels of sex hormones during puberty (Khairullah et al., 2014). We included the first 507 men who met these criteria and accepted the invitation to take part in the MRI substudy. Of these, 456 males completed all scanning using the same protocol (structural MRI, DTI, MTR and MWF); 51 participants completed the full protocol with a different DTI sequence. From this set, we excluded three participants who failed to pass quality control of the image-analysis pipeline. Quality control was based on successful registration of MR scans to T1w, and completion of cortical reconstruction by Freesurfer without any reported errors. The final sample analyzed for this report consisted of 453 (mean age of 19.6 years [standard deviation = 0.84 years])

2.2. MRI data acquisition

Magnetic resonance imaging (MRI) scans were acquired on a General Electric 3T HDx scanner with the following sequences; multicomponent driven equilibrium single pulse observation of T1 and T2 (mcDESPOT (Deoni et al., 2008)), magnetization transfer (MT) imaging, diffusion weighted imaging (DWI) and T1-weighted imaging. Details regarding the MR sequences have been described previously (Björholm et al., 2017). In brief, mcDESPOT was acquired using a 3D fast spoiled gradient recall (SPGR), with 8 T1-weighted SPGR, 2 inversion prepared SPGR and 15 T1/T2 weighted steady-state free precession images at a resolution of 1.72 x 1.72 x 1.70 mm. The DTI acquisition included 30 gradient directions with $b = 1200$ s/mm², and 3 ($b = 0$ s/mm²) non-diffusion weighted images with a resolution of 2.40 mm isotropic. MT imaging was acquired using a 3D SPGR scan with (MTon) and without (MToff) a magnetization radio-frequency off resonance pulse of 2 kHz, with a resolution of 1.90 mm isotropic. T1-weighted images were acquired at 1 mm isotropic using an inversion recovery fast SPGR sequence.

2.3. MRI data processing

T1w scans were processed through an automated cortical-reconstruction pipeline by FreeSurfer v6.0.0 (‘recon-all’). Imaging data acquired with mcDESPOT were preprocessed at Cardiff University Brain Research Imaging Centre; this involved fitting fast and slow relaxing water via the mcDESPOT model (Deoni et al., 2008). Magnetization transfer ratio (MTR) was calculated as follows (MToff – MTon)/MToff (Tofts, 2003). DWI maps underwent 1): correction for eddy current

distortion, 2) brain extraction, and 3) diffusion tensor imaging (DTI) model fitting using FSL's toolset 'eddy_correct', 'bet', and 'dtifit', respectively (Jenkinson et al., 2012). Quantitative T1, T2, MWF, MTR, synthetic T1w/T2w and the B0 DTI map were registered to native FreeSurfer space using 6-parameter linear registration followed by diffeomorphic intrasubject inter-modality registration from Advanced Normalization Tools (Avants et al., 2009). T1w/T2w are referred to as synthetic in this report as they are derived from modelling the mcDESPOT data rather than independent T1w and T2w acquisitions. FA and MD maps were registered to native FreeSurfer space using the transforms from the B0 registration above. MRI derived measures were sampled in the middle of the cerebral cortex (i.e., halfway between pial surface and gray-white matter boundary, Supplementary Figure 1); these single-voxel measures were averaged within each of the 34 cortical regions (left hemisphere) parcellated in the Desikan-Killiany atlas (Desikan et al., 2006). Statistical outliers were defined as $\pm 3SD$; a minimum of 439 participants contributed to each measure per region.

2.4. Virtual histology analysis

We use virtual histology to relate inter-regional variations in MRI measures to those in cell-specific gene expression; this method has been described previously (Shin et al., 2017), and employed in a number of other reports from our laboratory (Patel et al., 2018; Vidal-Pineiro et al., 2019). In short, we use gene-expression data obtained *post mortem* from the left hemisphere of six donors (24, 31, 39, 49, 55, 57 years of age), included in the Allen Human Brain Atlas (Hawrylycz et al., 2012). Expression data were mapped to the 34 regions of the Desikan-Killiany atlas used commonly in FreeSurfer (French and Paus, 2015). To ensure representativeness of the inter-regional profiles of gene expression across the 34 regions, we used only genes that passed the following two-stage consistency filter. In stage one, we retain only genes that have a donor-to-median correlation higher than 0.446 (threshold based on random simulation of donor profiles). In stage two, we retain only genes with a correlation of 0.52 or greater with another independent atlas of gene expression (BrainSpan Atlas; www.brainspan.org). The threshold of $r > 0.52$ corresponds to the one-sided test p -value < 0.05 for the correlation between the expression profiles from BrainSpan and the Allen Human Brain Atlas for a given gene. There were nine donors from the BrainSpan atlas (ages 13, 15, 18, 21, 23, 30, 36, 37, and 40 years), and included gene-expression data from 11 of the 34 cortical regions. After this two-stage filtering, only 2511 genes (out of the total of 20,737 genes) are retained, and used for virtual histology. Next, cell-specific genes are obtained from single-cell RNA sequencing of the mouse hippocampus and somatosensory cortex (Zeisel et al., 2015); these genes are intersected with the list of 2511 consistent genes. This resulted in the following number of genes per cell type: S1 pyramidal neurons ($n = 73$), CA1 pyramidal neurons ($n = 103$), interneurons ($n = 100$), astrocytes ($n = 54$), microglia ($n = 48$), oligodendrocytes ($n = 60$), ependymal ($n = 84$), endothelial ($n = 57$), and mural ($n = 25$). Lastly, the inter-regional profiles of a given MRI metric is correlated with inter-regional expression profiles of each of the cell-specific genes. The resulting distribution of correlation coefficients was tested for significance using a two-sided test with a resampled mean-centered null distribution from 100,000 iterations. To do this, we generate an empirical null distribution by randomly selecting the same number of genes as in a given cell type and their mean correlation coefficient is calculated. This is repeated for 100,000 iterations to make up the null distribution. The test statistic (average cell-specific correlation) is compared against the null distribution using a two-sided test.

All multiple comparisons within the report were corrected using False Discovery Rate (FDR) (Benjamini and Hochberg, 1995). Specifically, for virtual histology, FDR was applied for the 9 cell types tested for significance and for the 8 MR modalities tested within this report, thus correcting for a total of 72 multiple comparisons.

2.5. Gene ontology analysis

Gene ontology (GO) analysis was conducted on cell-specific gene sets that had at least one significant association with an MRI profile. GO was run using the enrichr toolkit (Kuleshov et al., 2016) using default settings (August 2019), and the top 25 GO terms for biological process, molecular function, and cellular compartment ontologies.

2.6. Variation of inter-regional multi-modal MRI profiles explained by cell types

The percent of variation of multi-modal MRI profiles explained by cell types was determined by R2 value from linear regression models. Each modality was modelled as a function of average cell-type expression profiles. The average cell-type expression profile was generated by averaging the expression of cell-specific genes following unit scaling across the 34 regions. For each linear model, average cell-type profiles were included as independent predictor variables if they were identified as significant from virtual histology analysis (above). Adjusted R2 value was used to estimate amount of variance explained after controlling for the effect of the number of independent predictors in a model. The following regression models were investigated:

$$\begin{aligned} \text{MWF} &= \text{CA1 Pyramidal} + \text{Astrocyte} + \text{Oligodendrocyte} \\ \text{Thick} &= \text{CA1} + \text{Astrocyte} \\ \text{T1} &= \text{CA1} + \text{Astrocyte} \\ \text{T2} &= \text{CA1} + \text{Astrocyte} + \text{S1} + \text{Oligodendrocyte} \\ \text{T1w/T2w} &= \text{CA1} + \text{Astrocyte} + \text{S1} + \text{Oligodendrocyte} \\ \text{FA} &= \text{CA1} + \text{Astrocyte} + \text{S1} \\ \text{MTR} &= \text{CA1} + \text{S1} \end{aligned}$$

2.7. Relative contribution of multi-modal MRI profiles in mean cell-specific profiles

To assess relative importance of different multi-modal MRI metrics in explaining average cell-specific profiles, we use the lmg measure (averaging over orders approach) in the "Relaimpo" R package (Grömping, 2006). This approach decomposes model-explained variance (R2) into non-negative contributions of each predictor/regressor in the presence of multi-correlated measures, and robust to order effects in a multivariable linear regression. Bootstrapping with 1000 replications were used to generate 95% confidence intervals of lmg estimates per regressor in a model. Difference in relative contribution between regressors in a model was tested using bootstrapped 95% confidence intervals. This was conducted using the command "boot.relimp". Confidence intervals for the bootstrapped intervals were used to determine nominal significance (relaimpo does not generate p values natively). Only cell types that showed at least one significant correlation from virtual histology with an MRI measure were used to assess relative contribution. The following regression models were investigated:

$$\begin{aligned} \text{Astrocyte} &= \text{Thickness} + \text{T1} + \text{T2} + \text{MWF} + \text{T1w/T2w} + \text{FA} \\ \text{CA1 Pyramidal} &= \text{Thickness} + \text{T1} + \text{T2} + \text{MWF} + \text{T1w/T2w} + \text{MTR} + \text{FA} \\ \text{S1 Pyramidal} &= \text{T2} + \text{T1w/T2w} + \text{MTR} + \text{FA} \\ \text{Oligodendrocyte} &= \text{T2} + \text{MWF} + \text{T1w/T2w} \end{aligned}$$

3. Results

Fig. 1 and Supplementary Figure 2 depict inter-regional variations in MR-based measures across the 34 cortical regions of the Desikan-Killiany atlas. Several of these measures correlate with one another across the 34 regions (Fig. 2).

Next, we correlate – across the 34 cortical regions – these MR-measures with cell-specific gene expression profiles (Table 1 and Fig. 3). Quantitative T1, T2, and FA are positively associated with CA1

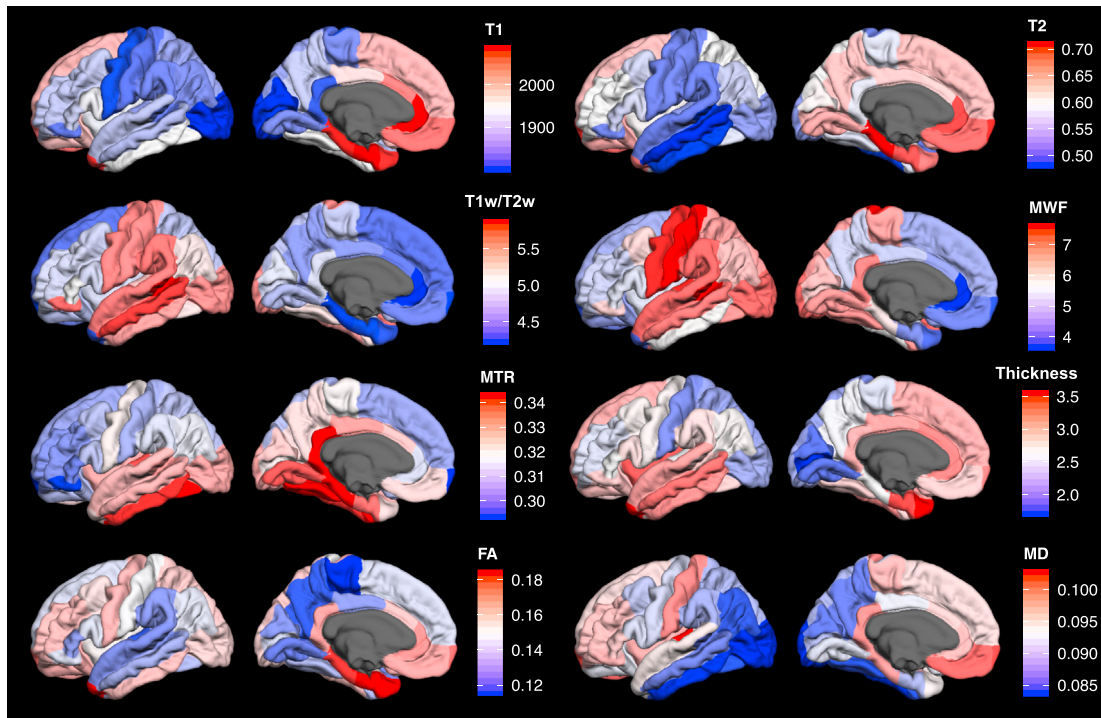


Fig. 1. Profiles of MR-derived measures across the left hemisphere of the cerebral cortex. Legend units: T1 (ms), T2 (ms), T1w/T2w = ratio of synthetic T1w and synthetic T2w, myelin water fraction (MWF), magnetization transfer ratio (MTR), Thickness (mm), fractional anisotropy (FA) and mean diffusivity (MD; $\text{mm}^2 \cdot \text{s}^{-1}$). T2, T1T2, MWF, and MD have been scaled up by a factor of 100. Color bars and look-up tables were generated through an automated script, where only maximum and minimum are used to set the extremes of the color bar.

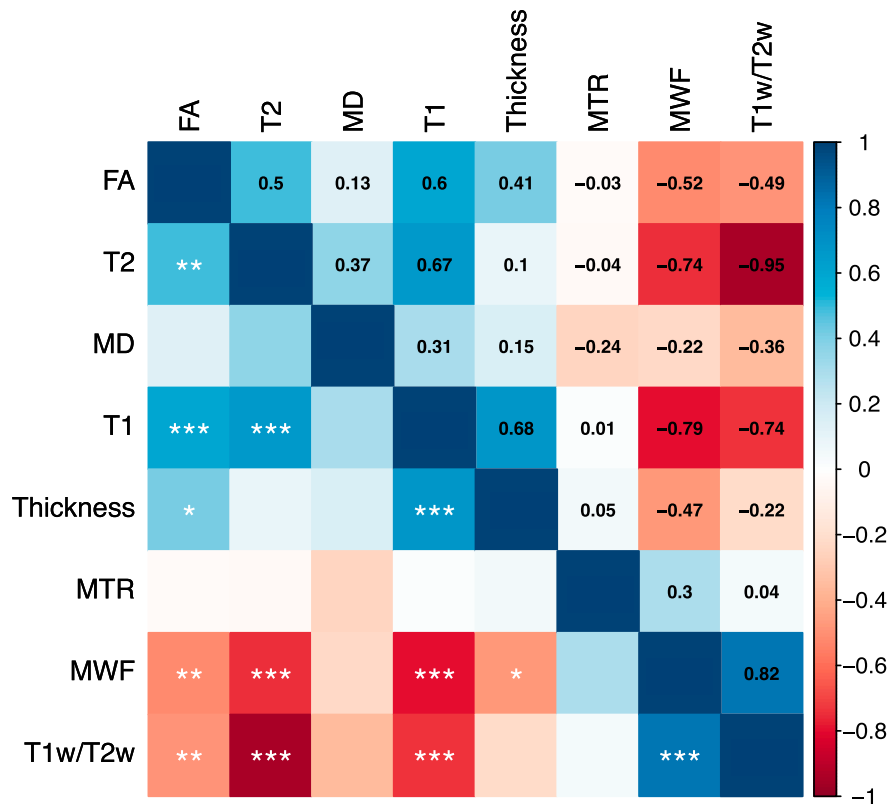


Fig. 2. Pearson correlation matrix between MR-derived measures across the 34 regions of the Desikan-Killiany atlas (left hemisphere only). Data are ordered via hierarchical clustering. Numbers and color shading represents Pearson correlation coefficient (r). * False Discovery Rate (FDR) < 0.05, ** < 0.01, *** < 0.001.

Table 1
Results from virtual histology.

Cell Type	MRI measures – average r (FDR p-value)							
	Thickness	qT1	qT2	MWF	MTR	T1w/T2w	MD	FA
Astrocyte	0.323 (1.68E-03)	0.313 (1.68E-03)	0.109 (1.17E-02)	-0.209 (2.74E-03)	0.047 (2.85E-01)	-0.162 (2.07E-03)	0.028 (4.12E-01)	0.225 (1.68E-03)
CA1 Pyramidal	0.287 (2.40E-04)	0.273 (2.40E-04)	0.118 (4.32E-04)	-0.181 (4.32E-04)	0.074 (7.87E-03)	-0.134 (4.80E-04)	0.044 (1.31E-01)	0.187 (2.40E-04)
Endothelial	-0.081 (5.97E-01)	-0.094 (5.97E-01)	-0.032 (5.97E-01)	0.057 (5.97E-01)	0.002 (9.88E-01)	0.028 (6.00E-01)	-0.029 (5.97E-01)	-0.056 (5.97E-01)
Ependymal	0.071 (4.67E-01)	0.121 (1.47E-01)	0.090 (5.38E-02)	-0.096 (1.33E-01)	0.068 (5.38E-02)	-0.095 (5.38E-02)	0.006 (8.72E-01)	0.087 (1.33E-01)
Interneuron	0.020 (7.48E-01)	0.025 (7.48E-01)	0.033 (7.43E-01)	-0.043 (7.43E-01)	-0.037 (7.43E-01)	-0.025 (7.48E-01)	0.026 (7.43E-01)	0.017 (7.48E-01)
Microglia	0.234 (6.62E-02)	0.244 (5.98E-02)	0.074 (1.24E-01)	-0.147 (7.41E-02)	0.009 (9.88E-01)	-0.105 (7.41E-02)	0.075 (1.24E-01)	0.185 (5.23E-02)
Mural	0.115 (6.79E-01)	0.115 (6.79E-01)	0.040 (6.79E-01)	-0.079 (6.79E-01)	0.013 (9.88E-01)	-0.052 (6.79E-01)	0.058 (6.79E-01)	0.047 (7.50E-01)
Oligodendrocyte	-0.112 (4.16E-01)	-0.147 (1.76E-01)	-0.130 (1.40E-02)	0.156 (4.36E-02)	0.000 (9.88E-01)	0.130 (2.54E-02)	-0.037 (4.16E-01)	-0.129 (5.92E-02)
S1 Pyramidal	-0.08 (4.67E-01)	-0.127 (1.76E-01)	-0.085 (4.93E-02)	0.068 (3.68E-01)	-0.085 (4.93E-02)	0.096 (4.93E-02)	0.000 (9.95E-01)	-0.124 (4.93E-02)

Table 1 Average correlation coefficients obtained by correlating (across the 34 regions) inter-regional profiles of expression of genes specific to 9 cell types with inter-regional profiles of various MRI measures. Means are corrected for the mean of the null distribution. T1w/T2w ratio is “synthetic” as it comes from the same mcDESPOT data as MWF with a different model fitting. False Discovery Rate (FDR) corrected P-values for 9 cell-type specific comparisons and 8 MRI modality comparisons in parentheses. *FDR-adjusted P-value < 0.05.

pyramidal ($r = 0.273$ [$p = 2.4E-04$], $r = 0.118$ [$p = 4.32E-04$], $r = 0.187$ [$p = 2.4E-04$], respectively) and astrocyte-specific gene expression ($r = 0.313$ [$p = 1.68E-03$], $r = 0.109$ [$p = 1.17E-02$], $r = 0.225$ [$p = 1.68E-03$], respectively); this is also the case for cortical thickness ($r = 0.287$ [$p = 2.40E-04$], $r = 0.323$ [$p = 1.68E-03$] for CA1 and astrocytes, respectively) as we observed previously in other MRI datasets (Shin et al., 2017)). MWF is associated with oligodendrocyte-specific gene expression ($r = 0.156$ [$p = 4.36E-02$]), while synthetic T1w/T2w ratio is associated with oligodendrocyte and S1 pyramidal specific gene expression ($r = 0.130$ [$p = 2.54E-02$], $r = 0.096$ [$p = 4.93E-02$], respectively). Both MWF and synthetic T1w/T2w ratio are negatively related with astrocyte ($r = -0.209$ [$p = 2.74E-03$], $r = -0.162$ [$p = 2.07E-03$], respectively) and CA1 pyramidal specific gene expression ($r = -0.181$ [$p = 4.32E-04$], $r = -0.134$ [$p = 4.8E-04$], respectively). Quantitative T2 is negatively associated with oligodendrocyte ($r = -0.130$ [$p = 1.40E-02$]) and S1 pyramidal specific gene expression ($r = -0.085$ [$p = 4.93E-02$]). MTR is associated with CA1 pyramidal-specific gene expression ($r = 0.074$ [$p = 7.87E-03$]); as we observed previously in other MRI datasets (Patel et al., 2018)) as well as negatively associated with S1 pyramidal cell specific gene expression ($r = -0.085$ [$p = 4.93E-02$]). MD is not correlated with any cell-specific gene expression profiles. Taken together, the identified cell types from virtual histology explain 67%, 63%, 47%, 45%, 39%, 37%, and 5% of variance in inter-regional profiles of MWF, cortical thickness, T1w/T2w ratio, T2, T1, FA, and MTR (Fig. 4).

We estimate the relative contributions of multi-modal MRI profiles to the explained variation in average cell-type profiles using relative importance metrics, ‘lmg’ (Fig. 5). Thickness and T1 had the highest relative contributions to the average astrocyte and CA1 pyramidal profiles. For astrocytes, thickness and T1 contributed 25.6% [CI, 10.0–39.5%] and 17.7% [CI, 7.8–27.1%] of variance, respectively. For CA1 pyramidal cells, thickness and T1 contributed 33.7% [17.3–46.4%] and 18.9% [CI, 7.76–29.6%], respectively. For oligodendrocytes, MWF, T2, and T1w/T2w contributed, respectively, 32.0% [CI, 20.0–44.0%],

17.7% [CI, 11.3–25.9%] and 16.6% [CI, 11.1–24.0%] to the variation in mean inter-regional expression.

Post hoc pairwise comparisons between the differences in relative importance revealed 15.4% [CI, 3.29–27.3%] greater contributions of MWF than T1w/T2w to explain the variation in mean oligodendrocyte profile (Supplemental Figure 3). This was also the case for thickness and less so for T1 when compared with other measures such as MWF, T1w/T2w, for astrocytes, and T2, MWF, MTR and FA for CA1 pyramidal (Supplemental Figure 3).

In order to distinguish features of the two pyramidal-cell types, gene ontology enrichment analysis reveals involvement of dendrite arbor/membrane related processes in the CA1 pyramidal gene set, and voltage-gated potassium channel activity related processes in the S1 pyramidal gene set (Supplementary Tables 1 and 2). Oligodendrocyte specific gene panel is enriched with cellular compartments related to axons, and biological processes related to phosphatidylinositol binding (Supplementary Table 3). There were no significant terms enriched within the astrocyte panel of genes following correction of multiple comparison although the top terms were related to metabolic processes (Supplementary Table 4).

4. Discussion

We present several associations between inter-regional variations in MRI measures and cell-specific gene expression profiles, demonstrating the potential for detecting certain neurobiological and cellular compartments of the cerebral cortex. MRI measures were correlated with one another (except for MTR; Fig. 2). It is therefore not surprising that virtual histology shows similar cell-specific correlates across these measures. Correlated inputs into virtual histology will produce correlated outputs, reflecting a lack of specificity of the MR measures. Inter-correlated MRI profiles, and consequently similar virtual-histology findings in general and CA1 pyramidal cells in particular, suggest shared neurobiology that varies systematically across the cortical ribbon. There are basic principles

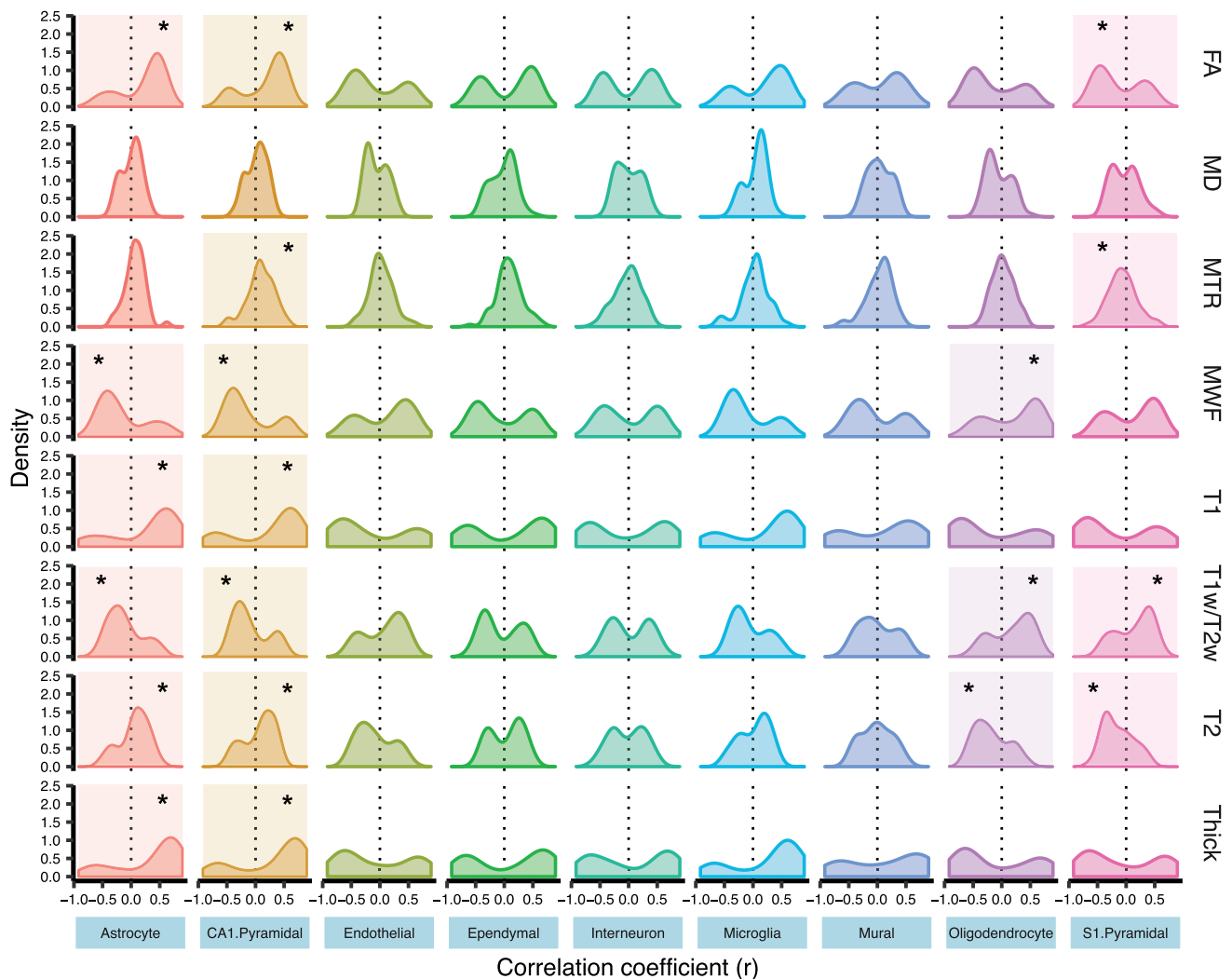


Fig. 3. Distribution of Pearson correlation coefficients between MRI-derived cortical profiles and profiles of expression of individual genes constituting the nine cell-specific panels. Significance of distribution from the null is calculated with a two-sided test. * False Discovery Rate (FDR) < 0.05 after correcting for 9 cell-type specific tests and 8 MRI profile tests (a total of 72 comparisons).

of cortical organization across lamina, and regions with distinct patterns of neuronal densities, dendritic complexity, connectivity and architectonic features (Barbas, 2015; Charvet et al., 2015). This is also reflected in the shared gradients of cytoarchitecture, interneuron densities, axonal connectivity, and MRI derived T1w/T2w within mouse cortex (Fulcher et al., 2019). It is possible that these MRI profiles are reflecting a common, systematic topological organization and, as such it is expected that neurons (CA1 pyramidal) and astrocytes (metabolically supporting glia) are underlying this commonality.

Although mean effect sizes from virtual histology are subtle ($0.074 < r < 0.323$), average cell-type expression profiles identified from virtual histology explain up to 67% variance for MWF across the 34 cortical regions, and as little as 5% for MTR. This variation demonstrates differences in the nature of these MRI measures and their sensitivity to certain neurobiological processes.

4.1. Quantitative T1, T2 and MWF

Inter-regional profiles of T1 and T2 relaxation times are highly correlated across the cerebral cortex, and both measures correlate negatively with MWF. This pattern is consistent with previous literature showing a similar relationship between T1 and T2 across the human

cerebral cortex (Larsson et al., 1986). Virtual histology revealed that T1 correlates positively with CA1 pyramidal, astrocyte, and microglia specific gene-expression profiles. This finding fits well with histologically measured correlates of T1 within the cerebral cortex. For example, intra-laminar variations in T1 are correlated with intra-laminar profiles reflecting myeloarchitecture (through myelin staining, and potentially capturing the trend we observe with oligodendrocyte-specific signal), and cytoarchitecture (cell-body staining, potentially capturing CA1 pyramidal and astrocyte signal observed in this report) (Eickhoff et al., 2005). Eickhoff and colleagues reported stronger correlations with myeloarchitecture, as compared with cytoarchitecture (Eickhoff et al., 2005). It is difficult, however, to compare these findings with those obtained here given the lack of laminar specificity in both *in vivo* MRI measures obtained in our sample and values of gene expression from the cerebral cortex (all laminae). Furthermore, there were only two regions (striate and extrastriate visual cortex) from four donors characterized in (Eickhoff et al., 2005). Likewise, histological examination of normal and pathological (focal cortical dysplasia) cortical tissue showed a positive correlation between neuronal MAP2 staining and T1 relaxation times ($R^2 = 0.26$), along with a negative correlation with myelin (SMI94/MBP) staining ($R^2 = 0.27$) (Reeves et al., 2016). The positive relationship between MAP2 (a prototypical marker of dendrites and cell bodies (Caceres

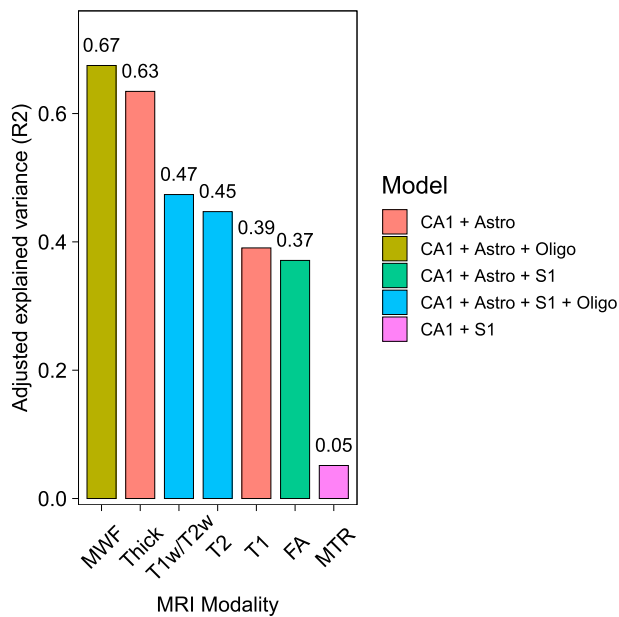


Fig. 4. Explained variance, R^2 , of MRI profiles by the average cell-type specific expression profiles identified from virtual histology. R^2 values estimated from a linear regression model including the specified cell types (legend color) included as independent regressors in the model. Average cell type profiles are generated through averaging scaled expression profiles for each of the cell specific genes for a given cell type. Adjusted R^2 values are used to account for differences in the number of cell types (regressors) across the various linear models.

et al., 1984)) and T1 relaxation time is consistent with the positive association we observe between inter-regional profiles of T1 relaxation time and gene expression specific to the CA1 pyramidal cells – a set of genes enriched in dendrite-related biological processes (Supplementary Table 1).

T2-relaxation profile was correlated negatively with the oligodendrocyte and S1-pyramidal gene-expression profiles; gene sets that are enriched, respectively, with axonal-related cellular compartment and voltage-gate potassium channel activity (Supplementary Tables 3 and 2). Given the unique function of oligodendrocytes in myelination in the central nervous system (Pérez-Cerdá et al., 2015), we interpret the oligodendrocyte-specific findings to be related to myelin-related processes. Furthermore, the pairing of S1 and oligodendrocyte may be due to the intimate relationship between neural activity (S1 pyramidal) and myelination (oligodendrocyte) (Fields, 2015). This interpretation is also consistent with previous histological studies that observed a strong negative correlation between T2 relaxation time and myelin content (MBP staining, $R^2 = 0.26$) across normal-appearing gray matter and lesion-containing cortical areas in *post mortem* samples from patients with multiple sclerosis (Tardif et al., 2012). T2 relaxation was also positively correlated with CA1 pyramidal- and astrocyte-specific gene expression. This relationship was also observed in normal cortical regions of interest between *ex vivo* T2 and immunolabelled MAP2 & glial fibrillary acid protein (GFAP), markers of neurons/dendrites and astrocytes, respectively (Reeves et al., 2016).

Lastly, MWF profile was correlated positively with that of the oligodendrocyte-specific gene panel, fitting well with previously described strong correlations between MWF and myelin staining (Luxol fast blue; mean $R^2 = 0.67$) across gray matter, white matter and lesion-containing cortical samples from 25 patients with multiple sclerosis (Laule et al.,

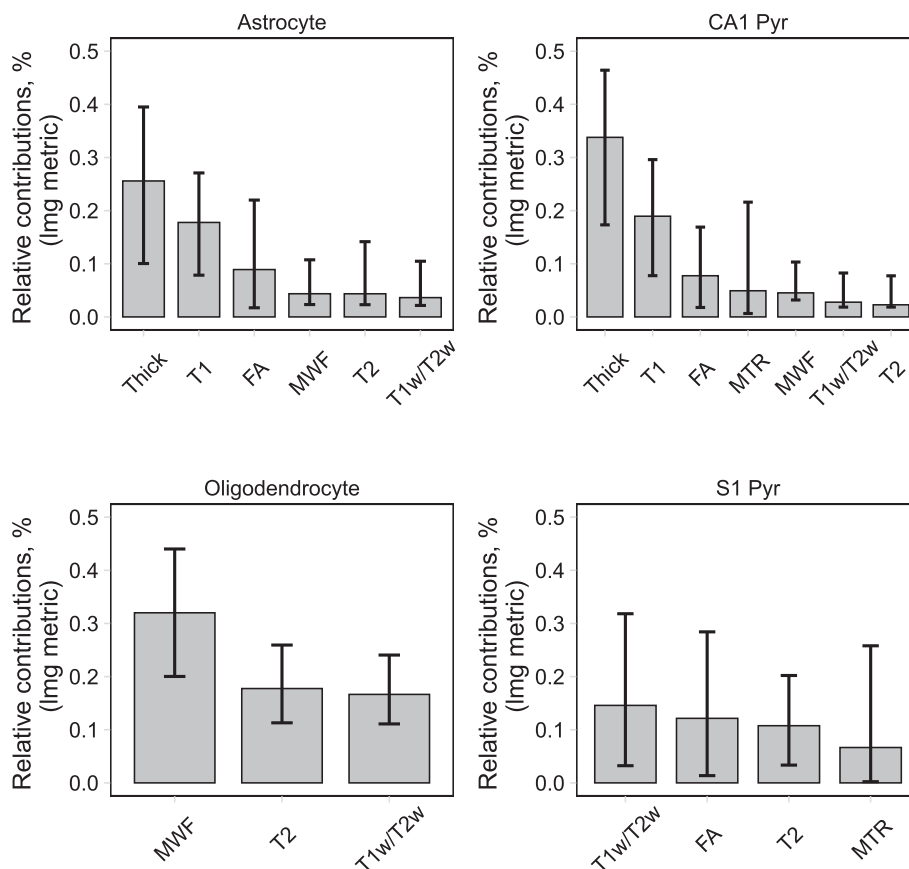


Fig. 5. Relative contribution (with 95% CI intervals) of inter-regional profiles of MRI measures to mean cell-specific expression profiles. Estimates are bootstrapped with 1000 replicates. Only cell type- and MR pairings that were significant from virtual histology are tested. ‘lmg’ metric decomposes model-explained variance (R^2) into non-negative contributions of each predictor/regressor. CA1 Pyr, CA1 Pyramidal cells; S1 Pyr, S1 Pyramidal cells.

2006). Given the strong negative correlation between MWF and T2 relaxation, is it not surprising that the MWF profiles were negatively associated with CA1 pyramidal and astrocytes. It is possible that regions with greater dendritic arborisation are also regions that happen to have less myelination (per unit of volume). For instance, dendritic trees were more complex (in terms of length and branching) in hetero-modal/supramodal areas (ex. Brodmann's area, BA10) as compared with primary and unimodal areas (ex. BA4,3,1,2) (Jacobs et al., 2001). On the other hand, primary and unimodal areas (BA4,3,1,2) exhibited the greatest amount of myelinated-fibre density while supramodal areas such as frontopolar (BA10) had the least amount of myelin from a wide age range donors (0–50 years) (Miller et al., 2012). These observations are from two independent reports with independent samples. This also may be a consequence of differences in water content given the positive association between T1, T2 relaxation and water content (Larsson et al., 1986). These are possible explanations for the observed relationship between CA1 pyramidal/astrocyte expression and several myelin-related measures in this report, such as T2, MWF, and T1w/T2w ratio. Regardless, cell types from virtual histology explained a majority of variation in the MWF profile ($R^2 = 0.67$), and the MWF profile contributes greater relative variation in mean oligodendrocyte-specific expression profile as compared with T1w/T2w when included in a multivariable linear model. This may suggest that MWF is more sensitive than T1w/T2w to oligodendrocyte-related profiles, and as an extension, to intracortical myelination.

4.2. Synthetic T1w/T2w ratio

The positive correlations – across the 34 regions - between T1w/T2w ratio and both MWF and oligodendrocyte-specific gene expression support the use of synthetic T1w/T2w ratio as a measure sensitive to intracortical myelination. Nonetheless, we caution the sole interpretation of T1w/T2w ratio as related to myelin as there may be other sources of signals potentially indicated by the observed correlation with the S1 pyramidal-specific genes. Additionally, it is important to consider that both the (synthetic) T1w/T2w ratio and MWF come from the same acquisition with a different model fit. An independent T1w and T2w acquisitions would be ideal to confirm this association. Histologically measured dendrite density was positively correlated with T1w/T2w ratio in *post mortem* samples from multiple sclerosis patients ($n = 9$) across five regions of the cerebral cortex (Righart et al., 2017). We observe an opposite association, inferred from the negative association between CA1 pyramidal (dendrite enriched gene set) and T1w/T2w profiles. Righart and colleagues also do not find an association between T1w/T2w ratio and myelin content, conflicting with the results from virtual histology. The main difference between our approach and the findings by Righart et al. is the state of the tissue: *in vivo* vs. *post mortem*. From Righart et al., one cannot rule out effects of fixation, partial volume effect from 3 mm slice thickness, and the inherent differences in tissue analyzed from late stage multiple sclerosis donors. Direct histological examinations in disease-free cortical samples between dendrite density (and other microstructural measures) and T1w/T2w ratio are warranted.

4.3. Magnetization transfer ratio

Inter-regional variations in MTR were correlated with CA1 pyramidal and S1 pyramidal specific gene expression. GO groups related to dendrite membrane and potassium channel activity are enriched in CA1 and S1 pyramidal gene sets, respectively (Supplementary Tables 1 and 2). This report replicates the association between MTR and CA1-pyramidal specific genes found in an independent dataset of adolescents from a subsample of the IMAGEN study (Patel et al., 2018). The ependymal-specific association with MTR, as reported previously (Patel et al., 2018), was not significant after correcting for the eight MRI profiles tested using virtual histology. As previously described, we interpret this association as related to inter-regional variations in the macromolecular content and

surface area of dendritic arbour and dendritic spines promoting efficient transfer of magnetization between the bound and free pool (Patel et al., 2018). MTR is not specific to dendrites (or myelin). The MT phenomena may occur in any large macromolecule with low molecular tumbling rate, making the measure sensitive to a variety of cellular processes (such as dendrites or myelin), but specific to virtually none. This is reflected in very minimal variance explained (5%) by mean CA1 and S1 pyramidal expression profiles. We caution against the use of MTR as a marker specific to myelin in gray matter; this interpretation does not take into account sources of MT signal from macromolecules other than those in myelin. This is also supported by the lack of an inter-regional relationship between MTR and MWF observed in this report, and by others in normal gray matter (Vavasour et al., 1998). Furthermore, histological quantification of myelin through staining of proteolipid protein in the cerebral cortex of mice did not correlate with MTR (Fjær et al., 2013). There are also reports demonstrating the opposite, a positive relationship between MTR and myelin from ex-vivo MRI samples across a variety of cortical regions (Reeves et al., 2016; Tardif et al., 2012). Note, however, that a majority of these inter-regional correlations were from samples from the frontal cortex as compared with our analysis that spans the entire neocortex. (Reeves et al., 2016) also showed opposite relationships with neuron density and MTR. It is difficult to compare MTR results as Reeves and colleagues used a 9.4T field strength scanner, and different saturation offset parameters as this report (6 kHz versus our 2 kHz); both of which are known to influence MT effects (Pohmann et al., 2011).

4.4. Diffusion tensor imaging

Through virtual histology, FA was correlated positively with CA1 pyramidal- and astrocyte-specific gene expression; it also correlated negatively with S1 pyramidal-specific gene expression profiles. This lack of specificity at a cellular level is in agreement of the prevailing view of FA being driven by multiple features, such as density and orientation of dendrites and axons. We speculate that regions with greater CA1 pyramidal and astrocytes have more organized neuronal efferent axons indexed by higher anisotropic diffusion of water.

4.5. Cortical thickness

We replicate the observed association between cortical thickness and CA1-pyramidal, and astrocyte- specific gene expression as shown previously in several different cohorts (Shin et al., 2017; Vidal-Pineiro et al., 2019). Microglia specific association with cortical thickness from the previous reports was nominally significant in this report. The CA1-pyramidal gene set is enriched in dendrite-arbor related processes, suggesting that regions with greater cortical thickness also have greater dendritic arborisation. We speculate that regions with more CA1 pyramidal cell-type signature would also require greater metabolic and homeostatic maintenance provided by astrocytes and microglia, respectively. Although there has yet to be a histological examination of inter-regional variation in cortical thickness and dendritic arbor, inter-individual differences in cortical thickness from samples of the temporal cortex correlate positively with histologically measured total dendritic length of pyramidal neurons in layers II/III (Goriounova et al., 2018). The relationship between thickness and dendrites is also reflected by the greatest relative contribution of cortical thickness on pyramidal (CA1) expression profile, as well on the astrocyte profile.

4.6. Neurobiologically driven selection of multi-modal sequences

The benefit of multi-modal acquisition in MRI-based studies is apparent (Mangeat et al., 2015; Warntjes et al., 2017); study protocols are, however, limited by time (length of MR session) and the cost associated with longer/multi-modal protocols. The associations derived from virtual histology may help in deciding which MRI sequences to acquire given specific neurobiological hypotheses of a study. For instance, if a

study aims to detect changes in (intracortical) myelination, a protocol including either quantitative T2, MWF, or T1w/T2w ratio may be warranted. From the relative contributions analysis, greater contribution to the oligodendrocyte expression profile is conferred by MWF as compared with T1w/T2w, potentially supporting the use of one measure over another.

4.7. Conflicting lines of evidence

There are several inconsistencies present between virtual-histology derived results and histological correlates from prior literature. T1 and MTR have been shown to correlate with myelin content through various histological (Reeves et al., 2016; Tardif et al., 2012), and MRI based approaches (Whitaker et al., 2016). We do not observe a significant association between oligodendrocyte-specific gene expression and T1 or MTR from virtual histology. Likewise, cortical T1w/T2w ratio was associated with dendrite density and not with myelin density in cortical pathological sections from multiple sclerosis patients (Righart et al., 2017). We see the opposite from virtual histology, a negative correlation with dendrite-related cell type (CA1) and a positive relationship with myelination (oligodendrocyte-related signal). On the other hand, the spatial variation in T1w/T2w across the cerebral cortex is correlated with independent maps of cortical myelination (Glasser and Van Essen, 2011). This may be due to methodological limitations of the virtual histology approach and/or methodological limitations from histological studies. Histological studies typically sample thin slices of tissue <20 μm increasing uncertainty in estimation of cellular compartments. Formalin fixation affects the MR properties of tissue, and biases myelin-sensitive sequences, altering correlates with ex-vivo histological measurements (Seifert et al., 2019; Shatil et al., 2018). The above issues highlight the need for large scale, multiplexed histological immunolabelling experiments where by a piece of tissue can be repeated be labelled with different markers (Murray et al., 2015). A holistic approach towards characterizing cortical structure, including cell types (neuron, astrocytes, microglia, etc.) and neuropil (dendrites, axons, glial processes, vasculature) all in the same piece of tissue may help shed light to these inconsistencies.

4.8. Limitations – sex bias

It is important to note that the results are from a sample of young men of a narrow age range (ages 18 to 21.5). This may limit generalisability of the results to the other sex and other ages. It should be noted, however, that MRI-cell type associations are unlikely to differ by sex when analysing inter-regional profiles in such a narrow age range. In our previous work using age-corrected cross-sectional data (adolescent samples), we observed very high correlations between inter-regional profiles of MRI measures between sexes ($r = 0.99$ for cortical thickness [Shin et al., 2017]; $r = 0.97$ for MTR [Patel et al., 2018]). Subtle sex differences were found only when analysing age-related variations (12–18 years of age) in MRI measures, including cortical thickness (Shin et al., 2017) or MTR (Patel et al., 2018). Overall, the profile-based approach is scale invariant and, as such, minimizes the effect any global differences across cortical regions. Nonetheless, subtle sex-related regional differences may remain after accounting for global variations (S. J. Ritchie et al., 2018) that may, in turn, influence the results from virtual histology.

4.9. Limitations – methodological

There are several methodological limitations to consider in the current report. Firstly, there is limited number of donors contributing to gene expression profiles from the Allen Human Brain Atlas ($n = 6$). This is partly mitigated by the two-stage filtering of genes, and using only those genes with high likelihood of their inter-regional profiles being representative.

Secondly, MR measures may be contaminated by the partial volume effect (PVE) given that the cortical sheet is rather thin (1–4 mm)

compared with the voxel sizes for the MR acquisitions analyzed in this report (mcDESPOT = $1.72 \times 1.72 \times 1.70$ mm, MTR = 1.9 mm isotropic, DTI = 2.4 mm isotropic). Partial volume effect may overestimate (or underestimate) some relationships observed in this report, such as the strong negative association between intra-cortical MWF and cortical thickness. Thicker regions are more likely to have a voxel capturing a bulk of the signal from the cerebral cortex, and less signal from its underlying white matter, which would have a very high MWF. On the other hand, thinner regions are more likely to be contaminated by signal from underlying white matter, making them appear to have more myelin. In some parts of the cerebral cortex, the chosen voxel resolution for MWF, MTR and diffusion-weighted imaging almost certainly results in PVE. Nonetheless, our cellular correlates of DTI measures (FA and MD) need to be appreciated with caution given the relatively large voxel size (2.4-mm isotropic), and consequently PVE especially in regions with low cortical thickness. In an effort to mitigate the effects of PVE, we sample from the middle of the cortex, half way between the gray-white boundary and the pial surface. There have been many different implementations of extracting intensity-based information from the cortex by weighting the midpoint of the cortical ribbon (Fukutomi et al., 2018; Glasser and Van Essen, 2011; Rowley et al., 2017). The commonality amongst all of them is to sample/weight intensity from the middle of the cortex. The rationale for this approach was also demonstrated by (Shafee et al., 2015) where voxels in the middle of the cerebral cortex were less likely to be contaminated (weighting factor ~ 1) and while voxels near the pial, and gray-white boundary surface were likely to be contaminated (weighting factor < 1).

Thirdly, values of MWF derived by mcDESPOT are known to be overestimated (Zhang et al., 2015) and, therefore, traditionally derived measures of MWF are required to corroborate findings reported here. It should be noted, however, that any global overestimation are unlikely to affect our conclusions as inter-regional profiles of MWF used in our analyses are scale invariant. Additionally there are concerns regarding parameter estimation in the mcDESPOT model (West et al., 2019). Lastly, MTR has been surpassed by a variety of other methods such as quantitative MT, and inhomogeneous MT, which allow for more accurate myelin estimation, as well as estimation of a variety of MT parameters such as magnetization transfer rate (Duhamel et al., 2019; Tofts, 2003).

Additionally, the cell-specific gene lists are derived from mouse single-cell RNA sequencing data. A majority of human RNA sequencing data are based on single-nucleus rather than single-cell RNA due to the methodological difficulties when working with human cells. Although there is general conservation between homologous mouse and human cell types, there are differences that may not be accounted for in this report (Hodge et al., 2019). Likewise, approximately 20–30% of genes do not have a one-to-one orthologous pair between humans and mouse (Breschi et al., 2017). A majority (87%) of cell-specific genes identified by (Zeisel et al., 2015) and used in this report have one-to-one homologous pairs, as identified by the NCBI homologue database. Single-cell data capture transcriptomic signals present within the soma and cellular projections (dendrites, axons, glial processes) while single-nucleus data are depleted of dendritically enriched transcripts (Skene et al., 2018). Given this, we have chosen to use mouse single-cell RNA sequencing for virtual histology analysis.

Finally, the chosen parcellation scheme (34 regions of Desikan-Killiany atlas) used for virtual histology may affect its ability to detect subtle regional variations in microstructure, and subtle correlates with cell types. This is reflected in the shared findings from MRI profiles, and virtual histology – capturing gross, systematic correlates across the cortical ribbon. Ritchie and colleagues applied a similar approach to this report, whereby T1w/T2w intensities at each vertex corresponding to the microarray samples from the Allen Human Brain Atlas are correlated (Ritchie et al., 2018). They find similar correlations between T1w/T2w and oligodendrocytes, CA1 pyramidal, and astrocyte-related expression. They also report correlations with microglia, and interneurons, and do not find associations with the S1 cell type, as reported here. This may be

due to methodological differences in MRI data (Human Connectome Project) and the lack of a consistency filter for selecting genes to be representative of the population (17,387 genes tested in the Ritchie report as compared with the 2511 'consistent' genes in this report). The Desikan-Killiany regional parcellation captures the gross correlates of MR measures across the cortical ribbon.

5. Conclusion

We provide consistent estimates of inter-regional variations in the cerebral cortex in a number of MR-derived measures, including T1 and T2 relaxation times, MWF, MTR, FA, and MD. These MR-based profiles map on unique and shared distributions of cell-specific gene-expression profiles. T2, Synthetic T1w/T2w ratio and MWF are correlated with oligodendrocyte-specific gene expression, supporting its use as a modality sensitive to myelin. MWF contributes greater explained variance in the oligodendrocyte profile when compared with T1w/T2w, potentially indicating its higher sensitivity for myelin. Lastly, cell-specific correlations and their relative contributions may help produce an initial framework for selecting MRI sequences to answer specific neurobiological questions within the cerebral cortex.

CRedit authorship contribution statement

Yash Patel: Formal analysis, Writing - review & editing. **Jean Shin:** Formal analysis. **Mark Drakesmith:** Formal analysis. **John Evans:** Formal analysis. **Zdenka Pausova:** Writing - review & editing. **Tomas Paus:** Writing - review & editing.

Acknowledgements

ALSPAC. We are grateful to all the families who took part in this study, and the whole ALSPAC team, which includes midwives, interviewers, computer and laboratory technicians, clerical workers, research scientists, volunteers, managers, receptionists and nurses. The UK Medical Research Council and Wellcome (Grant ref: 102215/2/13/2) and the University of Bristol provide core support for ALSPAC. This paper was supported by a grant from the National Institutes of Health (R01MH085772 to T. Paus). The content is solely the responsibility of the authors and does not necessarily represent the official views of the National Institutes of Health. Y. Patel is supported by an Alexander Graham Bell Canada Graduate Scholarship from the Natural Sciences and Engineering Research Council of Canada.

The code to perform virtual histology is provided at https://figshare.com/articles/Cell-specific_gene-expression_profiles_and_cortical_thickness_in_the_human_brain/4752955/3.

Appendix A. Supplementary data

Supplementary data to this article can be found online at <https://doi.org/10.1016/j.neuroimage.2020.116968>.

References

- Avants, B.B., Tustison, N., Song, G., 2009. Advanced normalization tools (ANTS). *Insight J* 2, 1–35.
- Barbas, H., 2015. General cortical and special prefrontal connections: principles from structure to function. *Annu. Rev. Neurosci.* 38, 269–289.
- Benjamini, Y., Hochberg, Y., 1995. Controlling the false discovery rate: a practical and powerful approach to multiple testing. *J. Roy. Stat. Soc. B* 57, 289–300.
- Bernhardt, B.C., Fadaie, F., de Wael, R.V., Hong, S.-J., Liu, M., Guiot, M.C., Rudko, D.A., Bernasconi, A., Bernasconi, N., 2018. Preferential susceptibility of limbic cortices to microstructural damage in temporal lobe epilepsy: a quantitative T1 mapping study. *Neuroimage* 182, 294–303.
- Björnholm, L., Nikkinen, J., Kiviniemi, V., Nordström, T., Niemelä, S., Drakesmith, M., Evans, J., Pike, G.B., Veijola, J., Paus, T., 2017. Structural properties of the human corpus callosum: multimodal assessment and sex differences. *Neuroimage* 152, 108–118.
- Boyd, A., Golding, J., Macleod, J., Lawlor, D.A., Fraser, A., Henderson, J., Molloy, L., Ness, A., Ring, S., Davey Smith, G., 2013. Cohort profile: the 'children of the 90s'—the index offspring of the Avon longitudinal study of Parents and children. *Int. J. Epidemiol.* 42, 111–127. <https://doi.org/10.1093/ije/dys064>.
- Braitenberg, V., Schüz, A., 2013. *Anatomy of the Cortex: Statistics and Geometry*. Springer Science & Business Media.
- Breschi, A., Gingeras, T.R., Guigó, R., 2017. Comparative transcriptomics in human and mouse. *Nat. Rev. Genet.* 18, 425.
- Caceres, A., Banker, G., Steward, O., Binder, L., Payne, M., 1984. MAP2 is localized to the dendrites of hippocampal neurons which develop in culture. *Dev. Brain Res.* 13, 314–318.
- Cercignani, M., Bozzali, M., Iannucci, G., Comi, G., Filippi, M., 2001. Magnetisation transfer ratio and mean diffusivity of normal appearing white and grey matter from patients with multiple sclerosis. *J. Neurol. Neurosurg. Psychiatr.* 70, 311–317.
- Charvet, C.J., Cahalane, D.J., Finlay, B.L., 2015. Systematic, cross-cortex variation in neuron numbers in rodents and primates. *Cerebr. Cortex* 25, 147–160.
- Chen, J.T.-H., Easley, K., Schneider, C., Nakamura, K., Kidd, G.J., Chang, A., Staugaitis, S.M., Fox, R.J., Fisher, E., Arnold, D.L., 2013. Clinically feasible MTR is sensitive to cortical demyelination in MS. *Neurology* 80, 246–252.
- De Boer, R.W., 1995. Magnetization transfer contrast. Part 1: MR Physics. *Philips Med. Syst.* 64–73.
- Deoni, S.C., Rutt, B.K., Arun, T., Pierpaoli, C., Jones, D.K., 2008. Gleaning multicomponent T1 and T2 information from steady-state imaging data. *Magn. Reson. Med.: Off. J. Int. Soc. Magn. Resonan. Med.* 60, 1372–1387.
- Desikan, R.S., Ségonne, F., Fischl, B., Quinn, B.T., Dickerson, B.C., Blacker, D., Buckner, R.L., Dale, A.M., Maguire, R.P., Hyman, B.T., 2006. An automated labeling system for subdividing the human cerebral cortex on MRI scans into gyral based regions of interest. *Neuroimage* 31, 968–980.
- Duhamel, G., Prevost, V., Cayre, M., Hertenau, A., Mchinda, S., Carvalho, V., Varma, G., Durbec, P., Alsop, D., Girard, O.M., 2019. Validating the sensitivity of inhomogeneous magnetization transfer (ihMT) MRI to myelin with fluorescence microscopy. *Neuroimage* 199, 289–303.
- Edwards, L.J., Kirilina, E., Mohammadi, S., Weiskopf, N., 2018. Microstructural imaging of human neocortex in vivo. *Neuroimage* 182, 184–206.
- Eickhoff, S., Walters, N.B., Schleicher, A., Kril, J., Egan, G.F., Zilles, K., Watson, J.D., Amunts, K., 2005. High-resolution MRI reflects myeloarchitecture and cytoarchitecture of human cerebral cortex. *Hum. Brain Mapp.* 24, 206–215.
- Fields, R.D., 2015. A new mechanism of nervous system plasticity: activity-dependent myelination. *Nat. Rev. Neurosci.* 16, 756–767.
- Fjær, S., Bø, L., Lundervold, A., Myhr, K.-M., Pavlin, T., Torkildsen, Ø., Wergeland, S., 2013. Deep gray matter demyelination detected by magnetization transfer ratio in the cuprizone model. *PLoS One* 8, e84162.
- Fjær, S., Bø, L., Myhr, K.-M., Torkildsen, Ø., Wergeland, S., 2015. Magnetization transfer ratio does not correlate to myelin content in the brain in the MOG-EAE mouse model. *Neurochem. Int.* 83, 28–40.
- Fraser, A., Macdonald-Wallis, C., Tilling, K., Boyd, A., Golding, J., Davey Smith, G., Henderson, J., Macleod, J., Molloy, L., Ness, A., Ring, S., Nelson, S.M., Lawlor, D.A., 2013. Cohort profile: the Avon longitudinal study of Parents and children: ALSPAC mothers cohort. *Int. J. Epidemiol.* 42 (1), 97–110. <https://doi.org/10.1093/ije/dys066>.
- French, L., Paus, T., 2015. A FreeSurfer view of the cortical transcriptome generated from the allen human brain atlas. *Front. Neurosci.* 9.
- Fukutomi, H., Glasser, M.F., Zhang, H., Autio, J.A., Coalson, T.S., Okada, T., Togashi, K., Van Essen, D.C., Hayashi, T., 2018. Neurite imaging reveals microstructural variations in human cerebral cortical gray matter. *Neuroimage* 182, 488–499.
- Fulcher, B.D., Murray, J.D., Zerbi, V., Wang, X.-J., 2019. Multimodal gradients across mouse cortex. *Proc. Natl. Acad. Sci. Unit. States Am.* 116, 4689–4695.
- Gelman, N., Ewing, J.R., Gorell, J.M., Spickler, E.M., Solomon, E.G., 2001. Interregional variation of longitudinal relaxation rates in human brain at 3.0 T: relation to estimated iron and water contents. *Magn. Reson. Med.: Off. J. Int. Soc. Magn. Resonan. Med.* 45, 71–79.
- Giedd, J.N., Blumenthal, J., Jeffries, N.O., Castellanos, F.X., Liu, H., Zijdenbos, A., Paus, T., Evans, A.C., Rapoport, J.L., 1999. Brain development during childhood and adolescence: a longitudinal MRI study. *Nat. Neurosci.* 2, 861.
- Glasser, M.F., Goyal, M.S., Preuss, T.M., Raichle, M.E., Van Essen, D.C., 2014. Trends and properties of human cerebral cortex: correlations with cortical myelin content. *Neuroimage* 93, 165–175.
- Glasser, M.F., Van Essen, D.C., 2011. Mapping human cortical areas in vivo based on myelin content as revealed by T1- and T2-weighted MRI. *J. Neurosci.* 31, 11597–11616.
- Goriounova, N.A., Heyer, D.B., Wilbers, R., Verhoog, M.B., Giugliano, M., Verbist, C., Obermayer, J., Kerkhofs, A., Smeding, H., Verberne, M., Idema, S., Baayen, J.C., Pieneman, A.W., de Kock, C.P., Klein, M., Mansvelter, H.D., 2018. Large and fast human pyramidal neurons associate with intelligence. *Elife* 7. <https://doi.org/10.7554/eLife.41714>.
- Gracien, R.-M., Reitz, S.C., Hof, S.M., Fleischer, V., Zimmermann, H., Droby, A., Steinmetz, H., Zipp, F., Deichmann, R., Klein, J.C., 2016. Changes and variability of proton density and T1 relaxation times in early multiple sclerosis: MRI markers of neuronal damage in the cerebral cortex. *Eur. Radiol.* 26, 2578–2586.
- Grömping, U., 2006. Relative importance for linear regression in R: the package relaimpo. *J. Stat. Software* 17, 1–27.
- Hawrylycz, M.J., Lein, E.S., Guillozet-Bongaarts, A.L., Shen, E.H., Ng, L., Miller, J.A., Van De Lagemaat, L.N., Smith, K.A., Ebbert, A., Riley, Z.L., 2012. An anatomically comprehensive atlas of the adult human brain transcriptome. *Nature* 489, 391.

- Hodge, R.D., Bakken, T.E., Miller, J.A., Smith, K.A., Barkan, E.R., Graybiel, L.T., Close, J.L., Long, B., Johansen, N., Penn, O., 2019. Conserved cell types with divergent features in human versus mouse cortex. *Nature* 573, 61–68.
- Huang, H., Yamamoto, A., Hossain, M.A., Younes, L., Mori, S., 2008. Quantitative cortical mapping of fractional anisotropy in developing rat brains. *J. Neurosci.* 28, 1427–1433.
- Jacobs, B., Schall, M., Prather, M., Kapler, E., Driscoll, L., Baca, S., Jacobs, J., Ford, K., Wainwright, M., Trembl, M., 2001. Regional dendritic and spine variation in human cerebral cortex: a quantitative golgi study. *Cerebr. Cortex* 11, 558–571.
- Jenkinson, M., Beckmann, C.F., Behrens, T.E., Woolrich, M.W., Smith, S.M., 2012. *Fsl*. *Neuroimage* 62, 782–790.
- Kamman, R., Go, K., Brouwer, W., Berendsen, H., 1988. Nuclear magnetic resonance relaxation in experimental brain edema: effects of water concentration, protein concentration, and temperature. *Magn. Reson. Med.* 6, 265–274.
- Khairullah, A., Klein, L.C., Ingle, S.M., May, M.T., Whetzel, C.A., Susman, E.J., Paus, T., 2014. Testosterone trajectories and reference ranges in a large longitudinal sample of male adolescents. *PLoS One* 9, e108838. <https://doi.org/10.1371/journal.pone.0108838>.
- Kuleshov, M.V., Jones, M.R., Rouillard, A.D., Fernandez, N.F., Duan, Q., Wang, Z., Koplev, S., Jenkins, S.L., Jagodnik, K.M., Lachmann, A., 2016. Enrichr: a comprehensive gene set enrichment analysis web server 2016 update. *Nucleic Acids Res.* 44, W90–W97.
- Larsson, E.-M., Englund, E., Györfy-Wagner, Z., Brun, A., Cronqvist, S., Persson, B., 1986. Regional differences in the proton magnetic resonance relaxation times T1 and T2 within the normal human brain. *Acta Radiol. Diagn.* 27, 231–234.
- Laule, C., Leung, E., Li, D.K., Traboulsee, A., Paty, D., MacKay, A., Moore, G.R., 2006. Myelin water imaging in multiple sclerosis: quantitative correlations with histopathology. *Multiple Sclerosis J.* 12, 747–753.
- Laule, C., Vavasour, I.M., Kolind, S.H., Li, D.K., Traboulsee, T.L., Moore, G.W., MacKay, A.L., 2007. Magnetic resonance imaging of myelin. *Neurotherapeutics* 4, 460–484.
- Lutti, A., Dick, F., Sereno, M.I., Weiskopf, N., 2014. Using high-resolution quantitative mapping of R1 as an index of cortical myelination. *Neuroimage* 93, 176–188.
- Mangeat, G., Govindarajan, S.T., Mainiero, C., Cohen-Adad, J., 2015. Multivariate combination of magnetization transfer, T2* and B0 orientation to study the myelo-architecture of the in vivo human cortex. *Neuroimage* 119, 89–102.
- Miller, D.J., Duka, T., Stimpson, C.D., Schapiro, S.J., Baze, W.B., McArthur, M.J., Fobbs, A.J., Sousa, A.M., Šestan, N., Wildman, D.E., 2012. Prolonged myelination in human neocortical evolution. *Proc. Natl. Acad. Sci. Unit. States Am.* 109, 16480–16485.
- Mori, S., Barker, P.B., 1999. *Diffusion Magnetic Resonance Imaging: its Principle and Applications*, vol. 257. The Anatomical Record: An Official Publication of the American Association of Anatomists, pp. 102–109.
- Murray, E., Cho, J.H., Goodwin, D., Ku, T., Swaney, J., Kim, S.-Y., Choi, H., Park, Y.-G., Park, J.-Y., Hubbert, A., 2015. Simple, scalable proteomic imaging for high-dimensional profiling of intact systems. *Cell* 163, 1500–1514.
- Ouyang, M., Jeon, T., Sotiras, A., Peng, Q., Mishra, V., Halovanic, C., Chen, M., Chalal, L., Rollins, N., Roberts, T.P., 2019. Differential cortical microstructural maturation in the preterm human brain with diffusion kurtosis and tensor imaging. *Proc. Natl. Acad. Sci. Unit. States Am.* 116 (10), 4681–4688, 201812156.
- Parry, A., Clare, S., Jenkinson, M., Smith, S., Palace, J., Matthews, P., 2003. MRI brain T1 relaxation time changes in MS patients increase over time in both the white matter and the cortex. *J. Neuroimaging* 13, 234–239.
- Patel, Y., Shin, J., Gowland, P., Pausova, Z., Paus, T., 2018. Maturation of the human cerebral cortex during adolescence: myelin or dendritic arbor? *Cerebr. Cortex* 29 (8), 3351–3362.
- Pérez-Cerdá, F., Sánchez-Gómez, M.V., Matute, C., 2015. Pío del Río Hortega and the discovery of the oligodendrocytes. *Front. Neuroanat.* 9, 92.
- Pohmann, R., Shajhan, G., Balla, D., 2011. Contrast at high field: relaxation times, magnetization transfer and phase in the rat brain at 16.4 T. *Magn. Reson. Med.* 66, 1572–1581.
- Preziosa, P., Kiljan, S., Steenwijk, M.D., Meani, A., van de Berg, W.D., Schenk, G.J., Rocca, M.A., Filippi, M., Geurts, J.J., Jonkman, L.E., 2019. Axonal degeneration as substrate of fractional anisotropy abnormalities in multiple sclerosis cortex. *Brain* 142 (7), 1921–1937.
- Reeves, C., Tachrount, M., Thomas, D., Michalak, Z., Liu, J., Ellis, M., Diehl, B., Miserocchi, A., McEvoy, A.W., Eriksson, S., 2016. Combined ex vivo 9.4 T MRI and quantitative histopathological study in normal and pathological neocortical resections in focal epilepsy. *Brain Pathol.* 26, 319–333.
- Righart, R., Biberacher, V., Jonkman, L.E., Klaver, R., Schmidt, P., Buck, D., Berthele, A., Kirschke, J.S., Zimmer, C., Hemmer, B., 2017. Cortical pathology in multiple sclerosis detected by the T1/T2-weighted ratio from routine magnetic resonance imaging. *Ann. Neurol.* 82, 519–529.
- Ritchie, J., Pantazatos, S.P., French, L., 2018a. Transcriptomic characterization of MRI contrast with focus on the T1-w/T2-w ratio in the cerebral cortex. *Neuroimage* 174, 504–517.
- Ritchie, S.J., Cox, S.R., Shen, X., Lombardo, M.V., Reus, L.M., Alloza, C., Harris, M.A., Alderson, H.L., Hunter, S., Neilson, E., 2018b. Sex differences in the adult human brain: evidence from 5216 UK biobank participants. *Cerebr. Cortex* 28, 2959–2975.
- Rowley, C.D., Sehmbi, M., Bazin, P., Tardif, C.L., Minuzzi, L., Frey, B.N., Bock, N.A., 2017. Age-related mapping of intracortical myelin from late adolescence to middle adulthood using T1-weighted MRI. *Hum. Brain Mapp.* 38, 3691–3703.
- Schmierer, K., Scaravilli, F., Altmann, D.R., Barker, G.J., Miller, D.H., 2004. Magnetization transfer ratio and myelin in postmortem multiple sclerosis brain. *Ann. Neurol.* 56, 407–415.
- Seifert, A.C., Umphlett, M., Hefti, M., Fowkes, M., Xu, J., 2019. Formalin tissue fixation biases myelin-sensitive MRI. *Magn. Reson. Med.* 82, 1504–1517.
- Shafiq, R., Buckner, R.L., Fischl, B., 2015. Gray matter myelination of 1555 human brains using partial volume corrected MRI images. *Neuroimage* 105, 473–485.
- Shatil, A.S., Uddin, M.N., Matsuda, K.M., Figley, C.R., 2018. Quantitative ex vivo MRI changes due to progressive formalin fixation in whole human brain specimens: longitudinal characterization of diffusion, relaxometry, and myelin water fraction measurements at 3T. *Front. Med.* 5, 31.
- Shin, J., French, L., Xu, T., Leonard, G., Perron, M., Pike, G.B., Richer, L., Veillette, S., Pausova, Z., Paus, T., 2017. Cell-specific gene-expression profiles and cortical thickness in the human brain. *Cerebr. Cortex* 1–11.
- Skene, N.G., Bryois, J., Bakken, T.E., Breen, G., Crowley, J.J., Gaspar, H.A., Giusti-Rodriguez, P., Hodge, R.D., Miller, J.A., Muñoz-Manchado, A.B., 2018. Genetic identification of brain cell types underlying schizophrenia. *Nat. Genet.* 1.
- Tardif, C.L., Bedell, B.J., Eskildsen, S.F., Collins, D.L., Pike, G.B., 2012. Quantitative magnetic resonance imaging of cortical multiple sclerosis pathology. *Multiple Sclerosis Int.* 2012.
- Thompson, P., Jahanshad, N., Ching, C.R., Salminen, L.E., Thomopoulos, S.I., Bright, J., Baune, B.T., Bertolin, S., Bralten, J., Bruin, W.B., 2019. ENIGMA and Global Neuroscience: A Decade of Large-Scale Studies of the Brain in Health and Disease across More than 40 Countries.
- Tofts, P., 2003. *Quantitative MRI of the Brain: Measuring Changes Caused by Disease*. Wiley, Chichester, West Sussex ; Hoboken, NJ.
- Tuor, U.I., Morgunov, M., Sule, M., Qiao, M., Clark, D., Rushforth, D., Foniok, T., Kirton, A., 2014. Cellular correlates of longitudinal diffusion tensor imaging of axonal degeneration following hypoxic-ischemic cerebral infarction in neonatal rats. *Neuroimage: Clinica* 6, 32–42.
- Uematsu, H., Popescu, A., Zhang, G., Wright, A.C., Wehrli, S.L., Takahashi, M., Wehrli, F.W., Selzer, M.E., Hackney, D.B., 2004. Magnetization transfer micro-MR imaging of live excised lamprey spinal cord: characterization and immunohistochemical correlation. *Am. J. Neuroradiol.* 25, 1816–1820.
- Vavasour, I.M., Whittall, K.P., Mackay, A.L., Li, D.K., Vorobeychik, G., Paty, D.W., 1998. A comparison between magnetization transfer ratios and myelin water percentages in normals and multiple sclerosis patients. *Magn. Reson. Med.* 40, 763–768.
- Vidal-Pineiro, D., Parker, N., Shin, J., French, L., Jackowski, A.P., Mowinckel, A.M., Patel, Y., Pausova, Z., Salum, G., Sorensen, O., 2019. Cellular Correlates of Cortical Thinning throughout the Lifespan, p. 585786 bioRxiv.
- Walhovd, K.B., Krogstad, S.K., Amlie, I.K., Bartsch, H., Bjørnerud, A., Due-Tønnessen, P., Grydeland, H., Hagler, D.J., Håberg, A.K., Kremen, W.S., 2016. Neurodevelopmental origins of lifespan changes in brain and cognition. *Proc. Natl. Acad. Sci. Unit. States Am.* 113, 9357–9362.
- Wartjes, J., Persson, A., Berge, J., Zech, W., 2017. Myelin detection using rapid quantitative MR imaging correlated to macroscopically registered luxol fast blue-stained brain specimens. *Am. J. Neuroradiol.* 38, 1096–1102.
- West, D.J., Teixeira, R.P., Wood, T.C., Hajnal, J.V., Tournier, J.-D., Malik, S.J., 2019. Inherent and unpredictable bias in multi-component DESPOT myelin water fraction estimation. *Neuroimage* 195, 78–88.
- Whitaker, K.J., Vértes, P.E., Romero-García, R., Váša, F., Moutoussis, M., Prabhu, G., Weiskopf, N., Callaghan, M.F., Wagstyl, K., Rittman, T., Tait, R., Ooi, C., Suckling, J., Inkster, B., Fonagy, P., Dolan, R.J., Jones, P.B., Goodyer, I.M., Bullmore, E.T., 2016. Adolescence is associated with genomically patterned consolidation of the hubs of the human brain connectome. *Proc. Natl. Acad. Sci. Unit. States Am.* 113, 9105–9110. <https://doi.org/10.1073/pnas.1601745113>.
- Zeisel, A., Muñoz-Manchado, A.B., Codeluppi, S., Lönnerberg, P., La Manno, G., Jureus, A., Marques, S., Munguba, H., He, L., Betsholtz, C., 2015. Cell types in the mouse cortex and hippocampus revealed by single-cell RNA-seq. *Science* 347, 1138–1142.